Catalysis Today 164 (2011) 520–527

Contents lists available at ScienceDirect

Catalysis Today

journal homepage: www.elsevier.com/locate/cattod

Influence of calcination temperature on iron titanate catalyst for the selective catalytic reduction of NO_x with NH_3

Fudong Liu [a], Kiyotaka Asakura [b], Hong He [a,*], Yongchun Liu [a], Wenpo Shan [a], Xiaoyan Shi [a], Changbin Zhang [a]

[a] State Key Laboratory of Environmental Chemistry and Ecotoxicology, Research Center for Eco-Environmental Sciences, Chinese Academy of Sciences, Beijing 100085, PR China
[b] Catalysis Research Center, Hokkaido University, Sapporo 001-0021, Japan

ARTICLE INFO

Article history:
Available online 18 November 2010

Keywords:
Selective catalytic reduction
Iron titanate catalyst
Calcination temperature
Intrinsic SCR activity
Thermal stability

ABSTRACT

The influence of calcination temperature on the microstructure, redox behavior, reactant adsorption capability and catalytic activity of iron titanate catalyst ($FeTiO_x$) for the selective catalytic reduction (SCR) of NO_x with NH_3 was investigated in detail using various characterization methods. After high temperature calcination (above 600 °C), the apparent SCR activity of $FeTiO_x$ catalyst obviously decreased, which was mainly due to decrease of surface area, pore volume, mobility of lattice oxygen and reactant adsorption capability. However, well crystallized pseudobrookite Fe_2TiO_5 showed much higher intrinsic SCR activity after normalization by surface area. This is mainly owing to the formation of larger proportion of monodentate nitrate, which is the real reactive nitrate species in the NO_x reduction process, among total nitrate species on the surface of $FeTiO_x$ catalysts with higher crystallization degree. This implies a possibility that the $FeTiO_x$ catalyst after high temperature calcination (600 or 700 °C) with higher thermal stability could be loaded onto porous support with large surface area to further improve its dispersion and thus the apparent SCR activity for practical use, such as the $DeNO_x$ process for diesel engines.

1. Introduction

Selective catalytic reduction (SCR) of NO_x with NH_3 is widely applied to the catalytic $DeNO_x$ process for stationary and mobile sources [1]. Nowadays, many researchers are interested in the development of new NH_3-SCR catalysts because of some inevitable disadvantages of the existing V_2O_5–WO_3 (MoO_3)/TiO_2 system in practical utilization, such as the narrow operation temperature window [2], the low N_2 selectivity at high temperatures, the high conversion of SO_2 to SO_3 [3] and the toxicity of vanadium pentoxide [4]. US has already preferred not to use vanadium-based SCR catalysts in the $DeNO_x$ process for mobile diesel engines [5,6].

Fe-based catalysts such as Fe/ZSM-5 [7–12], Fe/HBEA [13–16], Fe–TiO_2–PILC [17], Fe_2O_3/WO_3/ZrO_2 [18] and Fe–Mn/USY [19] usually show good SCR activity and N_2 selectivity, and TiO_2 is usually used as support for SCR catalysts because of its high resistance to SO_2 poisoning [20]. Under the consideration to combine the merits of Fe active component and TiO_2 support, in our previous study [21–23] we reported a novel and environmental-friendly iron titanate catalyst $FeTiO_x$ prepared by co-precipitation method, showing high NH_3-SCR activity, N_2 selectivity and H_2O/SO_2 durability in the medium temperature range (250–400 °C). However, the $FeTiO_x$ catalyst was mainly prepared at low calcination temperature, such as 400 °C, to obtain large surface area and pore volume, supplying more active sites for the SCR reaction and thus increasing the apparent SCR activity. In the practical utilization, such as the $DeNO_x$ process for diesel engines, the SCR reaction temperature may have sudden increase in some working conditions, resulting in the structural change and activity variation of $FeTiO_x$ catalyst. Therefore, it is very necessary to investigate the influence of calcination temperature on $FeTiO_x$ catalyst, which is also important for the further catalyst molding in practical use.

In this study, the microstructure of $FeTiO_x$ catalysts with different calcination temperatures was characterized by thermal gravity and differential thermal analysis (TG–DTA), N_2 physisorption, Fourier transform infrared absorption spectroscopy (FTIR absorption spectroscopy) and X-ray absorption fine structure spectroscopy (XAFS). The redox behavior of $FeTiO_x$ serial catalysts was investigated by X-ray photoelectron spectroscopy (XPS) plus H_2-temperature programmed reduction (H_2-TPR), and the reactant adsorption capability was evaluated using NH_3/NO_x-temperature programmed desorption (NH_3/NO_x-TPD) together with *in situ* diffuse reflectance infrared Fourier transform spectroscopy (*in situ* DRIFTS) of NH_3/NO_x adsorption. The experimental results in this study can supply some theoretical guidance for the optimization of preparation conditions and further industrial use of $FeTiO_x$ catalyst.

* Corresponding author at: P.O. Box 2871, 18 Shuangqing Road, Haidian District, Beijing 100085, PR China. Tel.: +86 10 62849123; fax: +86 10 62849123.
E-mail address: honghe@rcees.ac.cn (H. He).

0920-5861/$ – see front matter © 2010 Elsevier B.V. All rights reserved.
doi:10.1016/j.cattod.2010.10.008

2. Experimental

2.1. Catalyst synthesis and activity test

$FeTiO_x$ serial catalysts with different calcination temperatures (400, 500, 600 and 700 °C) were prepared by conventional co-precipitation method using $Fe(NO_3)_3{\cdot}9H_2O$ and $Ti(SO_4)_2$ as precursors with Fe–Ti molar ratio of 1:1 and $NH_3{\cdot}H_2O$ as precipitator, which are signed as $FeTiO_x$-400, 500, 600, 700 °C, respectively. The synthesis process has been described in detail in our previous study [21,22].

The steady state NH_3-SCR activity over $FeTiO_x$ serial catalysts was tested in a fixed-bed quartz tube reactor at atmospheric pressure, and the reaction conditions were controlled as follows: 500 ppm NO, 500 ppm NH_3, 5 vol.% O_2, N_2 balance; 0.6 ml catalyst, 20–40 mesh; total flow rate of 500 ml/min and gas hourly space velocity (GHSV) = 50 000 h^{-1}. The effluent gas was continuously analyzed using an FTIR spectrometer (Nicolet Nexus 670) equipped with a heated, low volume multiple-path gas cell (2 m).

The transient state NH_3-SCR activity over $FeTiO_x$ serial catalysts was investigated using temperature programmed surface reaction (TPSR) in SCR condition. A quadrupole mass spectrometer (HPR20, Hiden Analytical Ltd.) was used to record the signal of NO (m/z = 30). Prior to TPSR procedure, the catalysts (*ca.* 100 mg) were firstly pretreated at 300 °C for 0.5 h in a flow of 20 vol.% O_2/He (30 ml/min) and cooled down to the room temperature. Then the catalysts were exposed to a flow of 500 ppm NH_3 + 500 ppm NO + 5 vol.% O_2 (30 ml/min) for 1 h until the mass spectrometer signals were stabilized. Finally, the temperature was raised linearly to 500 °C at the rate of 10 °C/min in the same gas flow.

2.2. Characterizations

TG–DTA was conducted on a Shimadzu, DTG-60H apparatus to characterize the weight change and endothermal–exothermal status of $FeTiO_x$ catalyst precursor (precipitate after drying in air at 100 °C for 12 h) during the calcination procedure, then to infer the possible structural change and confirm the optimal catalyst calcination temperature. Before the measurement of TG–DTA curve, the $FeTiO_x$ catalyst precursor (*ca.* 10 mg) was pretreated in air condition at 120 °C for 1 h, and then cooled down to 30 °C holding for another 1 h. Finally, the temperature was raised linearly to 950 °C in air condition at the rate of 10 °C/min. During this process, the desorption of H_2O from $FeTiO_x$ catalyst precursor might occur, therefore we also conducted another H_2O-temperature programmed desorption (H_2O-TPD) experiment. Prior to the TPD procedure, the $FeTiO_x$ catalyst precursor (*ca.* 200 mg) was pretreated in a flow of 20 vol.% O_2/Ar (30 ml/min) at 120 °C for 1 h and then cooled down to the room temperature holding for another 1 h. In the same gas flow, the temperature was raised linearly to 950 °C at the rate of 10 °C/min. The H_2O signal (m/z = 18) was monitored on-line using the above-mentioned quadrupole mass spectrometer.

N_2 adsorption–desorption isotherms over $FeTiO_x$ serial catalysts were obtained at −196 °C using a Quantachrome Autosorb-1C instrument. Prior to N_2 physisorption, the catalysts were degassed at 300 °C for 4 h. Surface areas were determined by BET equation in 0.05–0.35 partial pressure range. Pore volumes, average pore diameters and pore size distributions were determined by Barrett–Joyner–Halenda (BJH) method from the desorption branches of the isotherms.

FTIR absorption spectroscopy was measured in a transmission mode with an FTIR spectrometer (Nicolet Nexus 670) equipped with a DTGS detector. The catalysts were diluted by KBr with the weight ratio of 1:8000 and then pressed into wafers. Using the KBr wafer as background, the spectra were collected in the range of 4000–400 cm^{-1} with a resolution of 4 cm^{-1}.

The XAFS including X-ray absorption near-edge spectroscopy (XANES) and extended X-ray absorption fine-structure spectroscopy (EXAFS) of Fe–K and Ti–K edges in $FeTiO_x$ serial catalysts were measured in a transmission mode at room temperature on BL-7C beam line, Photon Factory, Institute of Materials Structure Science (IMSS-KEK), Japan. The storage ring was operated at 2.5 GeV with 300 mA as an average storage current. The synchrotron radiation was monochromatized with a Si(1 1 1) double crystal monochromator, and mirrors were used to eliminate higher harmonics. The incident and transmitted beam intensities were monitored using ionization chambers filled with pure N_2. Data were analyzed using REX2000 program (Rigaku Co.). XANES were normalized with edge height. EXAFS oscillation $\chi(k)$ was extracted using spline smoothing with a Cook–Sayers criterion [24], and the filtered k^3-weighted $\chi(k)$ was Fourier transformed into R space (k range: 2.5–15 $Å^{-1}$ for Fe–K EXAFS and 2.5–13 $Å^{-1}$ for Ti–K EXAFS).

XPS was recorded on a Scanning X-ray Microprobe (PHI Quantera, ULVAC-PHI, Inc.) using Al K_α radiation. Binding energies of Fe 2p and Ti 2p were calibrated using C 1s peak (BE = 284.8 eV) as standard.

H_2-TPR experiments were carried out to investigate the influence of calcination temperature on the reducibility of $FeTiO_x$ serial catalysts. Prior to the TPR procedure, the catalysts (200 mg) were firstly pretreated in a flow of 20 vol.% O_2/Ar (30 ml/min) at 300 °C for 30 min and then cooled down to the room temperature. In a flow of 5 vol.% H_2/Ar (30 ml/min), the temperature was raised linearly to 900 °C at the rate of 10 °C/min. The H_2 signal (m/z = 2) was monitored on-line using the above-mentioned quadrupole mass spectrometer.

NH_3/NO_x-TPD experiments were performed on 200 mg catalysts using the above-mentioned quadrupole mass spectrometer to record the signals of NH_3 (m/z = 16) and NO_x (m/z = 30). Prior to the TPD procedure, the catalysts were pretreated at 300 °C for 0.5 h in a flow of 20 vol.% O_2/He (30 ml/min) and cooled down to the room temperature. Then the catalysts were exposed to a flow of 2500 ppm NH_3/Ar or 2500 ppm NO + 10 vol.% O_2/Ar (30 ml/min) for 1 h, following by Ar purge for another 1 h. Finally, the temperature was raised linearly to 500 °C in Ar flow at the rate of 10 °C/min.

The *in situ* DRIFTS experiments of NH_3/NO_x adsorption over $FeTiO_x$ catalysts were performed on an FTIR spectrometer (Nicolet Nexus 670) equipped with an MCT/A detector cooled by liquid nitrogen. An *in situ* DRIFTS reactor cell with ZnSe window (Nexus Smart Collector) connected to an adsorption/purging gas control system was used for NH_3/NO_x *in situ* adsorption experiments. The temperature of the reactor cell was controlled precisely by an Omega programmable temperature controller. Prior to NH_3/NO_x adsorption, the catalysts were pretreated at 400 °C in a flow of 20 vol.% O_2/N_2 for 0.5 h and cooled down to 30 °C. The spectra of different catalysts at 30 °C were collected in flowing N_2 and set as backgrounds, which were automatically subtracted from the final spectra after NH_3/NO_x adsorption. Then the catalysts were exposed to a flow of 500 ppm NH_3/N_2 or 500 ppm NO + 5 vol.% O_2/N_2 (300 ml/min) at 30 °C for 1 h, following by N_2 purge for another 0.5 h. All spectra were recorded by accumulating 100 scans with a resolution of 4 cm^{-1}.

3. Results and discussion

3.1. NH_3-SCR activity

Fig. 1 shows the steady state NH_3-SCR activity and TPSR results in SCR condition over $FeTiO_x$ catalysts with different calcination temperatures, based on which the influence of calcination temperature on the catalytic performance of $FeTiO_x$ catalysts can be fully investigated. From the results we can see that, with the

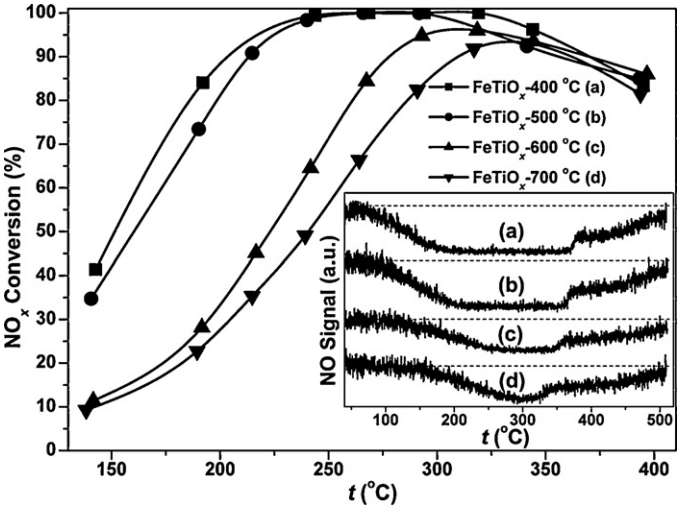

Fig. 1. Steady state NH_3-SCR activity and TPSR results over $FeTiO_x$ catalysts with different calcination temperatures.

increasing of calcination temperature, the steady state NO_x conversion showed an obvious decrease below 300 °C, and retained nearly the same above 300 °C. Comparing with $FeTiO_x$-400 °C catalyst, $FeTiO_x$-500 °C catalyst showed similar catalytic activity in the whole temperature range with NO_x conversion above 90% from 225 to 375 °C, while $FeTiO_x$-600 °C and $FeTiO_x$-700 °C catalysts showed much lower SCR activity in the low temperature range, indicating the possible severe structural change of $FeTiO_x$ catalysts after calcination at high temperatures (600 or 700 °C). As shown in Fig. S1, the NH_3 conversion in the SCR reaction over $FeTiO_x$ catalysts with different calcination temperatures followed nearly the same trend as that of NO_x conversion, while the N_2 selectivity showed some slight decrease with the increasing of catalyst calcination temperature. The TPSR results in the inset figure also shows that the temperature point to achieve the minimum NO concentration over $FeTiO_x$ catalysts after high temperature calcination was greatly delayed, and the catalyst operation temperature window was also narrowed, which is in well accordance with the steady state SCR activity test. In the following sections, we will fully investigate the influence of calcination temperature on the microstructure, redox behavior and reactant adsorption capability of $FeTiO_x$ catalyst using various characterization methods.

3.2. Structural property

3.2.1. TG–DTA and H_2O-TPD

Fig. 2 shows the TG–DTA curve and H_2O-TPD results of $FeTiO_x$ catalyst precursor. With the linear increasing of calcination temperature, the TG curve presented that the $FeTiO_x$ catalyst precursor showed an obvious weight loss due to the occurrence of dehydration effect. After calcination at 400 or 500 °C, the weight loss achieved 7.75%. Combining the DTA and H_2O-TPD results we can see that, the endothermal peak and H_2O desorption peak below 150 °C corresponded to the desorption of physisorbed H_2O. The three exothermal peaks and H_2O desorption peaks in the range of 200–360 °C corresponded to the desorption of H_2O produced by the acid–base neutralization reaction between basic hydroxyls in $Fe(OH)_x$ [25] and acidic hydroxyls in $Ti(OH)_x$ (orthotitanic acid or metatitanic acid) [26], in which process the iron titanate crystallite with specific Fe–O–Ti structure was formed. The endothermal peak and H_2O desorption peak in the range of 400–450 °C was due to the desorption of surface hydroxyls from iron titanate crystallite, which means that further increasing the calcination temperature could result in the decrease of surface Brønsted acid sites and thus the decrease of NH_3 adsorption amount in the SCR reaction condition. Above 600 °C, there was no H_2O desorption peak detected, and only an obvious endothermal peak was observed possibly due to the catalyst crystallization or phase transformation/separation. From 500 to 800 °C, the weight loss of $FeTiO_x$ catalyst precursor was only 0.60%, which might be caused by the decomposition of residual sulfate species from $Ti(SO_4)_2$ precursor.

3.2.2. N_2 physisorption

Fig. S2 shows the N_2 adsorption–desorption isotherms and pore size distributions of $FeTiO_x$ serial catalysts. For $FeTiO_x$-400 °C catalyst, the isotherm at low P/P_0 resembled closely with type IV isotherm according to the IUPAC classification [27], which is typical for mesoporous materials. However, at high P/P_0 the isotherm shifted from type IV to type II pattern, indicating the presence of some macropores in this sample. In addition, the hysteresis loop exhibited typical H3 type, revealing the slit-shaped pore structure in this catalyst [27]. With the increasing of calcination temperature, the N_2 adsorbed volume per weight showed an obvious decrease, and the closure point of hysteresis loop also moved to the higher P/P_0, indicating that much more macropores were formed after high temperature calcination. The pore size distributions also show that with the increasing of calcination temperature, the ratios of micropores and mesopores in $FeTiO_x$ catalysts were continuously decreased, and eventually mainly mesopores and macropores existed after 600 or 700 °C calcination.

Table 1 shows the structural parameters of $FeTiO_x$ catalysts with different calcination temperatures derived from N_2 physisorption results and the SCR reaction rates normalized by surface areas. After high temperature calcination, both surface area and pore volume showed an obvious decrease and the average pore diameter showed an evident increase, which is an important reason for the decline of apparent SCR activity. However, after normalization by surface areas, the SCR reaction rates over $FeTiO_x$ catalysts with high temperature calcination (600 or 700 °C) were much higher than those over $FeTiO_x$ catalysts with low temperature calcination (400 or 500 °C), which shows that well crystallized iron titanate catalyst also showed outstanding SCR activity due to the possession of Fe–O–Ti structure, although the amount of Fe–O–Ti structure exposed on the catalyst surface was greatly lowered due to the occurrence of crystallization or phase transformation. In practical use, such as the $DeNO_x$ process for diesel engine exhaust, the operation temperature of SCR catalyst might have some sudden increase in some working conditions, and $FeTiO_x$ catalysts with high calcination temperatures will be more appropriate to be utilized for this

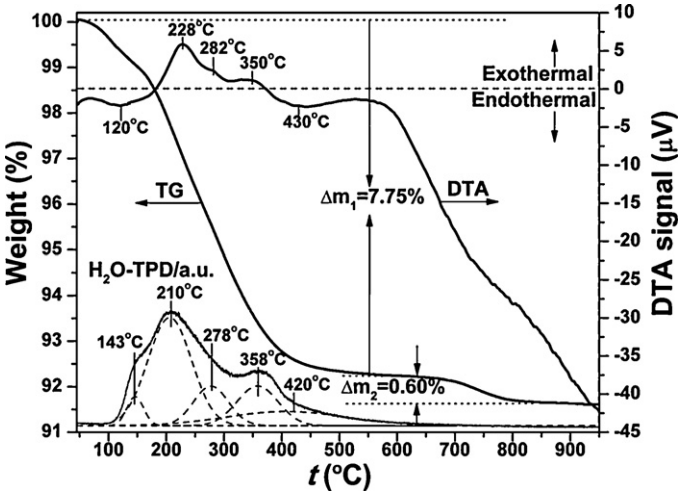

Fig. 2. TG–DTA curve and H_2O-TPD results of $FeTiO_x$ catalyst precursor.

Table 1
Structural parameters of $FeTiO_x$ catalysts with different calcination temperatures and SCR reaction rates normalized by surface areas.

Catalysts	S_{BET}[a] ($m^2\ g^{-1}$)	Pore volume[b] ($cm^3\ g^{-1}$)	Pore diameter[c] (nm)	Reaction rates at 150 °C[d] (10^{-10} mol s^{-1} m^{-2})
$FeTiO_x$-400 °C	245.3	0.52	8.3	8.83 (48% $DeNO_x$)
$FeTiO_x$-500 °C	150.6	0.47	12.2	11.82 (42% $DeNO_x$)
$FeTiO_x$-600 °C	48.3	0.37	30.7	12.06 (14% $DeNO_x$)
$FeTiO_x$-700 °C	28.1	0.30	43.2	15.83 (12% $DeNO_x$)

[a] BET surface area.
[b] BJH desorption pore volume.
[c] Average pore diameter.
[d] SCR reaction rates normalized by catalyst surface area (the "*x*% $DeNO_x$" in parentheses indicates the NO_x conversion at 150 °C for the calculation of SCR reaction rates over different $FeTiO_x$ catalysts).

process due to their higher thermal stability. To further increase the apparent SCR activity, it is possible to load $FeTiO_x$ catalysts after high temperature calcination (600 or 700 °C) onto porous support with large surface area to improve their dispersion and thus increase the number of active sites for the SCR reaction.

3.2.3. FTIR absorption spectroscopy

The XRD results in our previous study showed that the $FeTiO_x$-400 °C catalyst was mainly in the form of iron titanate crystallite with no obvious diffraction peaks, and with the increasing of calcination temperature from 500 to 700 °C, well crystallized pseudobrookite Fe_2TiO_5 and rutile TiO_2 were formed [21]. Fig. 3 shows the FTIR absorption spectroscopy of $FeTiO_x$ catalysts with different calcination temperatures measured in a transmission mode, which can supply more information about the microstructure of $FeTiO_x$ serial catalysts. As we can see, all samples showed the FTIR absorption bands at 3421 and 1635 cm^{-1}, which are attributed to surface hydroxyls and adsorbed H_2O, respectively. With the increasing of calcination temperature, especially to 600 or 700 °C, the band intensity of O–H stretching vibration mode at 3421 cm^{-1} showed some decrease, implying the occurrence of dehydroxylation effect and thus the decrease of surface Brønsted acid sites, which is in well accordance with the TG–DTA results. In the fundamental vibration region, only a broad band centered at 561 cm^{-1} was observed for $FeTiO_x$-400 °C catalyst, which probably can be ascribed to the multiple absorptions of Fe–O, Ti–O and Fe–O–Ti groups. Increasing the calcination temperature to 600 °C resulted in the splitting of this broad band into two sub-bands at 615 and 492 cm^{-1}, and further increasing to 700 and 800 °C resulted in the formation of three distinct sub-bands, which implies that the microstructure of $FeTiO_x$ catalysts showed obvious change during the calcination process. Among the three sub-bands, the bands at 808 and 661 cm^{-1} were attributed to the fundamental vibrations of Fe_2TiO_5 [28], and the band at 503 or 507 cm^{-1} was attributed to the fundamental vibration of Ti–O group in rutile TiO_2 [29]. No fundamental vibration of Fe–O group in Fe_2O_3 was observed [30], which is in well accordance with our previous XRD results [21].

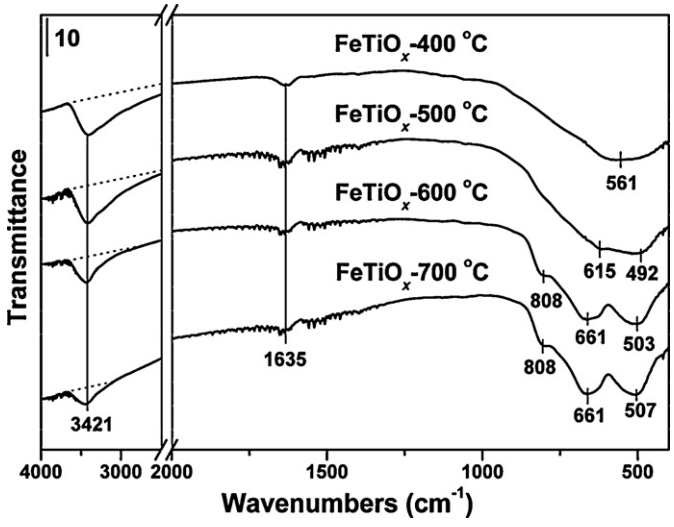

Fig. 3. FTIR absorption spectroscopy of $FeTiO_x$ catalysts with different calcination temperatures.

3.2.4. XAFS

Fig. 4 shows the XAFS results of $FeTiO_x$ catalysts with different calcination temperatures. As the XANES results in Fig. 4A and C shown, both of the pre-edge peaks of Fe–K and Ti–K edges in $FeTiO_x$ serial catalysts showed an obvious decrease in intensity with the increasing of calcination temperature. Our previous study already showed that the pre-edge peak intensity in XANES spectra was positively correlated with the structural distortion of specific element [22,31]. For example, smaller pre-edge peak intensity implied that well crystallized coordination shell existed around the target element. Therefore, the XANES results in this study indicate that the coordination structures of both Fe species and Ti species were transformed from severely distorted octahedron to more symmetrical octahedron, which is closely associated with the increasing of crystallization degree after high temperature calcination.

Fig. 4B and D shows the Fourier transforms of filtered EXAFS oscillations $k^3 \cdot \chi(k)$ of Fe–K and Ti–K edges in $FeTiO_x$ serial catalysts into *R* space. As we concluded in our previous study [22], the first coordination peaks of Fe–K and Ti–K edges in $FeTiO_x$-400 °C catalyst were ascribed to Fe–O and Ti–O coordination shells, and the second single coordination peaks were ascribed to Fe–O–Ti and Ti–O–Fe coordination shells. The weak intensity of the second coordination peaks implies that the $FeTiO_x$-400 °C catalyst was mainly in the form of iron titanate crystallite with specific Fe–O–Ti structure containing abundant structural defects, which is beneficial to the adsorption and activation of reactants in the SCR reaction. With the increasing of calcination temperature, the first coordination peaks of Fe–K and Ti–K edges showed no obvious change, however, the second single coordination peaks gradually split into two groups of sub-bands, with higher peak intensity and larger bond distance. According to the previous XRD results [21] and above-mentioned FTIR absorption spectroscopy, the sub-bands of Fe–K edge mainly consisted of Fe–O–Ti and Fe–O–Fe bonds from Fe_2TiO_5, and the sub-bands of Ti–K edge mainly consisted of Ti–O–Fe, Ti–O–Ti bonds from Fe_2TiO_5 and Ti–O–Ti bond from rutile TiO_2. The larger bond distance of Fe–O–Ti or Ti–O–Fe structure arose by high temperature calcination might result in the weakening of the interaction between Fe and Ti species to a certain extent. Although the high temperature calcination resulted in the severe change of the second coordination shells, the Fe–O–Ti or Ti–O–Fe structure (*i.e.* the first sub-band with higher intensity) was still present in well crystallized Fe_2TiO_5, continuing to perform high specific catalytic activity in the SCR reaction. Summarizing the TG–DTA, N_2 physisorption, FTIR absorption spectroscopy and XAFS results, it is concluded that

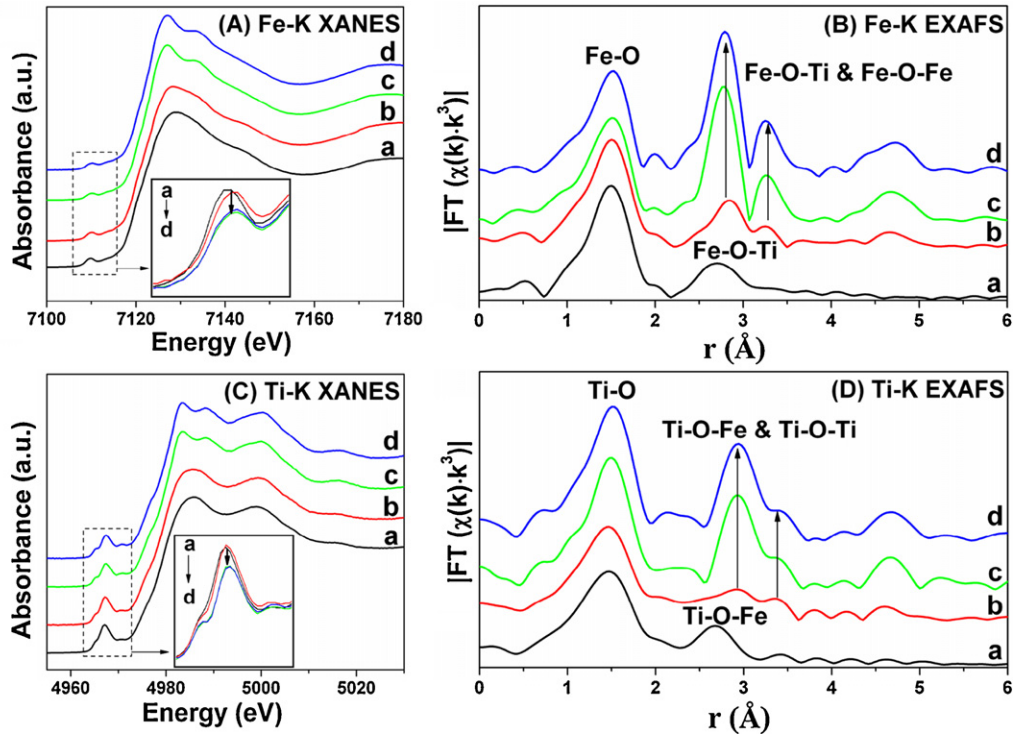

Fig. 4. XAFS results of $FeTiO_x$ catalysts with different calcination temperatures: (a) $FeTiO_x$-400 °C; (b) $FeTiO_x$-500 °C; (c) $FeTiO_x$-600 °C; (d) $FeTiO_x$-700 °C.

the high temperature calcination led to the enhancement of crystallization degree of $FeTiO_x$ catalyst, together with the decrease of surface area, pore volume, surface Brønsted acid sites, the number of structural defects and thus the apparent SCR activity.

3.3. Redox behavior

3.3.1. XPS

Fig. S3 shows the XPS results of $FeTiO_x$ catalysts with different calcination temperatures. As shown in Fig. S3A, the binding energies of Fe $2p_{3/2}$ (711.2 eV) and Fe $2p_{1/2}$ (724.9 eV) in $FeTiO_x$ serial catalysts corresponded well with those of Fe^{3+} [32,33], and no obvious change of Fe 2p binding energies was observed after high temperature calcination. In our previous study [22,23], we concluded that there was an electronic inductive effect between Fe^{3+} and Ti^{4+} species resulting in the enhancement of oxidative ability of Fe^{3+} species, and in this study the high temperature calcination did not change this situation. This result means that the surface Fe^{3+} species still showed high oxidative ability after high temperature calcination owing to the preservation of Fe–O–Ti structure in well crystallized Fe_2TiO_5. As shown in Fig. S3B, the binding energies of Ti $2p_{3/2}$ (458.6 eV) and Ti $2p_{1/2}$ (464.2 eV) in $FeTiO_x$-400 °C and $FeTiO_x$-500 °C catalysts were typical characteristics of Ti^{4+} [32,33], and after 600 or 700 °C calcination the binding energies of these two peaks shifted to 458.8 and 464.4 eV mainly due to the separation of partial rutile TiO_2 without strong electronic interaction with Fe^{3+} species. Summarizing the Fe 2p and Ti 2p XPS results we can see that, the apparent SCR activity decline of $FeTiO_x$ catalysts after high temperature calcination was not caused by the binding energy change of active Fe^{3+} species, but due to the high crystallization degree of pseudobrookite Fe_2TiO_5 accompanied by the separation of partial rutile TiO_2 and thus the decrease of catalytic active sites.

3.3.2. H_2-TPR

To further elucidate the influence of calcination temperature on the reducibility of $FeTiO_x$ serial catalysts, we also conducted H_2-TPR experiments and the results are shown in Fig. 5. To better understand the reduction process of Fe^{3+} species, the overlapped H_2 reduction peaks were deconvoluted into several sub-bands by searching for the optimal combination of Gaussian bands with the correlation coefficients (r^2) above 0.99 without fixing the sub-band positions (PeakFit software package, Version 4.12, SeaSolve Software Inc.). The sub-bands are signed as *a*, *b*, *c* from low to high temperatures, in which *a* donates the reduction of surface oxygen, *b* donates the reduction of Fe^{3+} to $Fe^{(3-\delta)+}$ ($\delta = 1/3$) and *c* donates the further reduction of $Fe^{(3-\delta)+}$ to Fe^{2+} plus partial Fe^0. b_1, b_2, c_1, and c_2 sub-bands refer to the reduction of iron species in different oxide layers of $FeTiO_x$ serial catalysts, such as the surface layer (b_1, c_1) and the bulk layer (b_2, c_2). According to our previous study [22,23], all Fe^{3+} species in $FeTiO_x$-400 °C catalyst can be reduced to Fe^{2+} by H_2 below 500 °C, and partial Fe^{2+} species can be further reduced to metallic Fe^0 above 500 °C. The area ratio of sub-

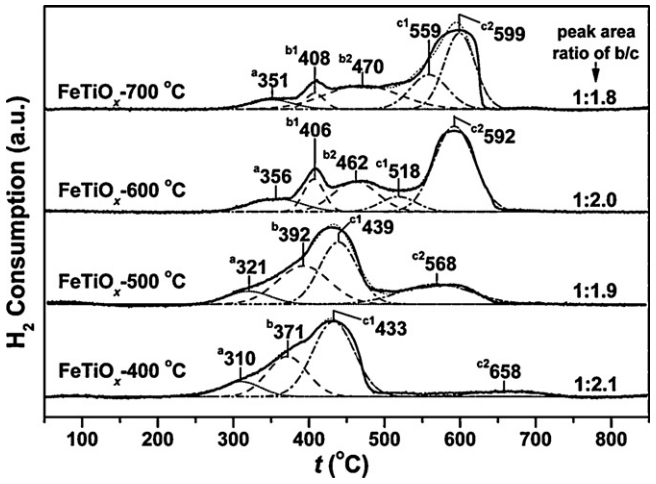

Fig. 5. H_2-TPR results of $FeTiO_x$ catalysts with different calcination temperatures.

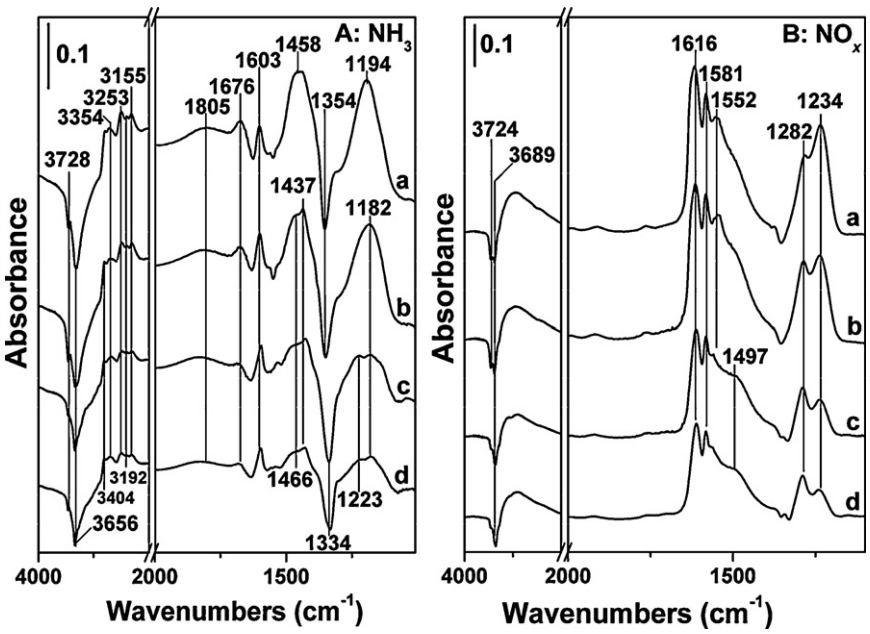

Fig. 6. *In situ* DRIFTS results of (A) NH_3 and (B) NO_x adsorption on $FeTiO_x$ catalysts with different calcination temperatures: (a) $FeTiO_x$-400 °C; (b) $FeTiO_x$-500 °C; (c) $FeTiO_x$-600 °C; (d) $FeTiO_x$-700 °C.

bands *b*/*c* (1:2.1) on $FeTiO_x$-400 °C catalyst in the present study is in well accordance with our previous conclusion. With the increasing of calcination temperature, the reduction temperature of surface oxygen (sub-bands *a*) was increased to a certain extent, and the reduction process of Fe^{3+} species also showed obvious variation. Remarkably, the sub-bands *b* and *c* shifted to the high temperature region, and more iron species was reduced in the bulk layer when the $FeTiO_x$ catalysts were calcined at high temperatures. For example, a majority of iron species in $FeTiO_x$-600 °C and $FeTiO_x$-700 °C catalysts was largely reduced around 600 °C. Although the Fe^{3+} species in all $FeTiO_x$ catalysts can be reduced to Fe^{2+} below 800 °C based on the area ratio of sub-bands *b*/*c* (1:1.8 ∼ 1:2.1), the reducibility of the catalysts after high temperature calcination was actually lowered. This means that the mobility of lattice oxygen was greatly weakened in this process, which is possibly associated with the inhibition of H_2 diffusion into the bulk phase of $FeTiO_x$ catalysts with high crystallization degree after high temperature calcination. The weakening of the mobility of lattice oxygen made a majority of Fe^{3+} species firmly confined in the crystal structure of $FeTiO_x$ catalysts, which was not beneficial to the accomplishment of redox cycle between Fe^{3+} and Fe^{2+}, thus leading to the decrease of low temperature apparent SCR activity.

3.4. Reactants adsorption capability

3.4.1. NH_3/NO_x-TPD

In NH_3-SCR reaction, especially in the low temperature range, both of NH_3 and NO_x can adsorb onto the catalyst surface and participate into the NO_x reduction process, therefore, we conducted NH_3/NO_x-TPD experiments over $FeTiO_x$ serial catalysts and the results are shown in Fig. S4. As the NH_3-TPD results shown in Fig. S4A, there were three groups of NH_3 desorption peaks detected over all samples, among which the peaks between 50 and 80 °C were attributed to the desorption of physisorbed NH_3, the peaks between 100 and 130 °C to the desorption of NH_4^+ bound to weak Brønsted acid sites [34,35], and the peaks above 200 °C to the multiple desorption of NH_4^+ bound to strong Brønsted acid sites plus coordinated NH_3 bound to Lewis acid sites [36]. With the increasing of calcination temperature, the total desorption amount of NH_3 over $FeTiO_x$ serial catalysts showed an obvious and monotonic decrease, and the desorption ratio of NH_4^+ bound to Brønsted acid sites also showed some decrease to a certain extent. This result indicates that besides of the decline of NH_3 adsorption amount caused by the decrease of surface area after high temperature calcination, the number of Brønsted acid sites was also decreased due to the dehydroxylation effect, which is in well accordance with the above-mentioned TG–DTA results and FTIR absorption spectroscopy. Our previous study showed that ionic NH_4^+ was the main active adsorbed NH_3 species in the SCR reaction at low temperatures [37], therefore, the SCR activity decline over $FeTiO_x$ catalysts after high temperature calcination was closely associated with the decrease of surface Brønsted acid sites.

As the NO_x-TPD results shown in Fig. S4B, there were three groups of NO_x desorption peaks detected over all samples, among which the peaks below 160 °C was ascribed to the decomposition of monodentate nitrate, the peaks between 200 and 270 °C to the decomposition of bridging nitrate, and the peaks between 320 and 330 °C to the decomposition of bidentate nitrate [23,31,37]. With the increasing of calcination temperature, the total desorption amount of NO_x over $FeTiO_x$ serial catalysts also showed an obvious and monotonic decrease, which was caused by the decrease of surface areas. Except the increasing of the decomposing temperature of bridging nitrate species over $FeTiO_x$ catalysts after high temperature calcination (from 203 to 261 °C), no obvious variation of thermal stability was observed for other nitrate species. It is noticeable that with the increasing of calcination temperature, only the band intensity of bridging nitrate and bidentate nitrate showed obvious decrease, yet the band intensity of monodentate nitrate kept constant. Therefore, the adsorption ratio of NO_x as monodentate nitrate was actually enhanced in this process, which might be relevant with the increasing of intrinsic SCR activity over $FeTiO_x$-600 °C and $FeTiO_x$-700 °C catalysts.

3.4.2. *In situ* DRIFTS of NH_3/NO_x adsorption

To investigate the surface adsorbed species after NH_3 or NO_x adsorption, we carried out the *in situ* DRIFTS experiments of NH_3/NO_x adsorption on $FeTiO_x$ serial catalysts with different calcination temperatures, and the results are presented in Fig. 6. After

NH_3 adsorption and N_2 purge, as shown in Fig. 6A, the catalyst surface was mainly covered by ionic NH_4^+ bound to Brønsted acid sites (1676 cm^{-1} and 1437–1466 cm^{-1}) [38,39] and coordinated NH_3 bound to Lewis acid sites (1603 cm^{-1} and 1182–1223 cm^{-1}) [39,40]. At the same time, the bands attributed to N–H stretching vibration modes at 3100–3400 cm^{-1}, the hydroxyl consumption bands at 3728 and 3656 cm^{-1} due to the interaction between NH_3 and surface acidic hydroxyls, and the negative bands at 1334–1354 cm^{-1} caused by the coverage of residual sulfate species from $Ti(SO_4)_2$ precursor by NH_3 also showed up. With the increasing of calcination temperature, both of the bands attributed to ionic NH_4^+ and coordinated NH_3 showed an obvious decrease in intensity, which is directly correlated with the decrease of surface acidic hydroxyls (*i.e.* Brønsted acid sites) and surface oxygen defects (*i.e.* Lewis acid sites) during the crystallization process.

As shown in Fig. 6B, after NO_x adsorption and N_2 purge, the catalyst surface was mainly covered by monodentate nitrate (1497–1552 cm^{-1} and 1282 cm^{-1}), bridging nitrate (1616 and 1234 cm^{-1}) and bidentate nitrate (1581 cm^{-1}), and the hydroxyl consumption bands at 3724 and 3689 cm^{-1} due to the interaction between surface basic hydroxyls and NO_x also showed up [41–45]. With the increasing of calcination temperature, the total adsorption amount of the three kinds of nitrate species showed obvious decrease, which is in well accordance with the NO_x-TPD results. However, it is noticeable that, although the absolute adsorption amount of monodentate nitrate on $FeTiO_x$ catalysts after high temperature calcination was decreased, the relative adsorption amount of monodentate nitrate among the three kinds of nitrate species was obviously increased. For instance, on $FeTiO_x$-600 °C and $FeTiO_x$-700 °C catalysts, the band intensity of ν_3 low vibration mode of monodentate nitrate at 1282 cm^{-1} was even higher than that of bridging nitrate at 1234 cm^{-1}. In our previous study [23], we have already concluded that monodentate nitrate was the real active NO_x adsorbed species in NH_3-SCR reaction at low temperatures. Due to the strong adsorption of NH_3 onto $FeTiO_x$ catalyst surface, the low temperature SCR activity was directly correlated to the adsorption amount of monodentate nitrate. Therefore, in this study, the increase of the SCR reaction rates normalized by surface areas over $FeTiO_x$ catalysts after high temperature calcination was mainly due to the enhancement of the relative adsorption amount of monodentate nitrate among total nitrate species on catalyst surface.

In short summary, after high temperature calcination (600 or 700 °C), the well crystallized $FeTiO_x$ catalysts with low surface area and pore volume would have smaller amount of surface acid sites and lower mobility of lattice oxygen (*i.e.* redox ability between Fe^{3+} and Fe^{2+}), which was not beneficial to the adsorption and activation of NH_3 or NO_x, thus leading to the decrease of apparent SCR activity. However, the adsorption of NO_x as highly reactive monodentate nitrate was actually enhanced to a certain extent after high temperature calcination, thus resulting in the increase of intrinsic SCR activity. In future preparation process of $FeTiO_x$ catalyst for practical use, the three factors for controlling the SCR activity including redox ability of Fe species, surface acidity and adsorption capability of monodentate nitrate can be adjusted and balanced by tuning the calcination temperatures.

4. Conclusions

The calcination temperature in the preparation process showed obvious influence on the microstructure, redox behavior, reactant adsorption capability of the $FeTiO_x$ serial catalysts and thus the relevant NH_3-SCR activity. After high temperature calcination (600 or 700 °C), well crystallized pseudobrookite Fe_2TiO_5 appeared in $FeTiO_x$ catalyst, leading to the decrease of surface area, pore volume, the mobility of lattice oxygen, the reactant adsorption capability and thus the apparent SCR activity. However, $FeTiO_x$-600 °C or $FeTiO_x$-700 °C catalyst showed higher thermal stability and intrinsic SCR activity after normalization by surface area, which is closely associated with the formation of larger proportion of monodentate nitrate among total nitrate species on catalyst surface. In the future study, $FeTiO_x$ catalysts after high temperature calcination can be loaded onto porous support with large surface area to further improve their dispersion and thus the apparent SCR activity in practical use.

Acknowledgements

This work was partially supported by the National High Technology Research and Development Program of China (2009AA064802 and 2009AA06Z301), the National Natural Science Foundation of China (50921064), the Photon Factory, KEK, Japan (Project No. 2009G177) and JSPS, Japan (Frontier Human Resources Development Project: Creation of Sustainable Catalysts for the New 21st Society).

Appendix A. Supplementary data

Supplementary data associated with this article can be found, in the online version, at doi:10.1016/j.cattod.2010.10.008.

References

[1] H. Bosch, F. Janssen, Catal. Today 2 (1988) 369.
[2] G. Busca, L. Lietti, G. Ramis, F. Berti, Appl. Catal. B: Environ. 18 (1998) 1.
[3] J.P. Dunn, P.R. Koppula, H.G. Stenger, I.E. Wachs, Appl. Catal. B: Environ. 19 (1998) 103.
[4] Vanadium Pentoxide, MSDS No. V2220, Mallinckrodt Baker, Phillipsburg, NJ, July 1, 2009. http://www.jtbaker.com/msds/englishhtml/v2220.htm (accessed 20.01.10).
[5] R. Baker, M. Block, Diesel Construction Equipment Database and NO_x Control Technology Evaluation for Houston, Final Report for Texas Environmental Research Consortium-New Technology Research and Development Program, 2007.
[6] S.-S. Adolf, P. Marcus, S. Paul, D. Yvonne, K. Thomas, L. Egbert, US Patents US2005/0196333A0196331 (2005).
[7] M. Schwidder, M.S. Kumar, A. Brückner, W. Grünert, Chem. Commun. (2005) 805.
[8] M. Devadas, O. Kröcher, M. Elsener, A. Wokaun, G. Mitrikas, N. Söger, M. Pfeifer, Y. Demel, L. Mussmann, Catal. Today 119 (2007) 137.
[9] M. Iwasaki, K. Yamazaki, K. Banno, H. Shinjoh, J. Catal. 260 (2008) 205.
[10] A.Z. Ma, W. Grünert, Chem. Commun. (1999) 71.
[11] R.Q. Long, R.T. Yang, J. Am. Chem. Soc. 121 (1999) 5595.
[12] J. Li, R. Zhu, Y. Cheng, C.K. Lambert, R.T. Yang, Environ. Sci. Technol. 44 (2010) 1799.
[13] A. Frey, S. Mert, J. Due-Hansen, R. Fehrmann, C. Christensen, Catal. Lett. 130 (2009) 1.
[14] M. Høj, M.J. Beier, J.-D. Grunwaldt, S. Dahl, Appl. Catal. B: Environ. 93 (2009) 166.
[15] P. Balle, B. Geiger, S. Kureti, Appl. Catal. B: Environ. 85 (2009) 109.
[16] P. Balle, B. Geiger, D. Klukowski, M. Pignatelli, S. Wohnrau, M. Menzel, I. Zirkwa, G. Brunklaus, S. Kureti, Appl. Catal. B: Environ. 91 (2009) 587.
[17] R.Q. Long, R.T. Yang, J. Catal. 186 (1999) 254.
[18] N. Apostolescu, B. Geiger, K. Hizbullah, M.T. Jan, S. Kureti, D. Reichert, F. Schott, W. Weisweiler, Appl. Catal. B: Environ. 62 (2006) 104.
[19] Q. Lin, J. Li, L. Ma, J. Hao, Catal. Today 151 (2010) 251.
[20] F. Nakajima, I. Hamada, Catal. Today 29 (1996) 109.
[21] F. Liu, H. He, C. Zhang, Chem. Commun. (2008) 2043.
[22] F. Liu, H. He, C. Zhang, Z. Feng, L. Zheng, Y. Xie, T. Hu, Appl. Catal. B: Environ. 96 (2010) 408.
[23] F. Liu, H. He, J. Phys. Chem. C 114 (2010) 16929.
[24] J.W. Cook, D.E. Sayers, J. Appl. Phys. 52 (1981) 5024.
[25] J. Baltrusaitis, J.H. Jensen, V.H. Grassian, J. Phys. Chem. B 110 (2006) 12005.
[26] S. Matsuda, A. Kato, Appl. Catal. 8 (1983) 149.
[27] K.S.W. Sing, D.H. Everett, R.A.W. Haul, L. Moscou, R.A. Pierotti, J. Rouquerol, T. Siemieniewska, Pure Appl. Chem. 57 (1985) 603.
[28] http://rruff.info/pseudobrookite/names/asc (accessed 20.06.10).
[29] S.K. Samantaray, T. Mishra, K.M. Parida, J. Mol. Catal. A: Chem. 156 (2000) 267.
[30] B. Pal, M. Sharon, G. Nogami, Mater. Chem. Phys. 59 (1999) 254.
[31] F. Liu, H. He, Y. Ding, C. Zhang, Appl. Catal. B: Environ. 93 (2009) 194.
[32] E.P. Reddy, L. Davydov, P.G. Smirniotis, J. Phys. Chem. B 106 (2002) 3394.
[33] S. Roy, B. Viswanath, M.S. Hegde, G. Madras, J. Phys. Chem. C 112 (2008) 6002.
[34] L.S. Cheng, R.T. Yang, N. Chen, J. Catal. 164 (1996) 70.

[35] R.Q. Long, R.T. Yang, J. Catal. 207 (2002) 158.
[36] L. Chmielarz, R. Dziembaj, T. Grzybek, J. Klinik, T. Łojewski, D. Olszewska, A. Węgrzyn, Catal. Lett. 70 (2000) 51.
[37] F. Liu, H. He, C. Zhang, W. Shan, X. Shi, Catal. Today, this issue.
[38] N.-Y. Topsøe, Science 265 (1994) 1217.
[39] F. Liu, H. He, Catal. Today 153 (2010) 70.
[40] G. Ramis, M.A. Larrubia, G. Busca, Top. Catal. 11–12 (2000) 161.
[41] Z. Liu, P.J. Millington, J.E. Bailie, R.R. Rajaram, J.A. Anderson, Micropor. Mesopor. Mater. 104 (2007) 159.
[42] G. Piazzesi, M. Elsener, O. Kröcher, A. Wokaun, Appl. Catal. B: Environ. 65 (2006) 169.
[43] W.S. Kijlstra, D.S. Brands, E.K. Poels, A. Bliek, J. Catal. 171 (1997) 208.
[44] W.S. Kijlstra, D.S. Brands, H.I. Smit, E.K. Poels, A. Bliek, J. Catal. 171 (1997) 219.
[45] G.M. Underwood, T.M. Miller, V.H. Grassian, J. Phys. Chem. A 103 (1999) 6184.